Evolution of carbon sinks in a changing climate

Inez Y. Fung*†, Scott C. Doney‡, Keith Lindsay§, and Jasmin John*

*Berkeley Atmospheric Sciences Center, University of California, Berkeley, CA 94720-4767; ‡Department of Marine Chemistry and Geochemistry, Woods Hole Oceanographic Institution, Woods Hole, MA 02543; and §National Center for Atmospheric Research, P.O. Box 3000, Boulder, CO 80307

Contributed by Inez Y. Fung, June 13, 2005

Climate change is expected to influence the capacities of the land and oceans to act as repositories for anthropogenic CO_2 and hence provide a feedback to climate change. A series of experiments with the National Center for Atmospheric Research–Climate System Model 1 coupled carbon–climate model shows that carbon sink strengths vary with the rate of fossil fuel emissions, so that carbon storage capacities of the land and oceans decrease and climate warming accelerates with faster CO_2 emissions. Furthermore, there is a positive feedback between the carbon and climate systems, so that climate warming acts to increase the airborne fraction of anthropogenic CO_2 and amplify the climate change itself. Globally, the amplification is small at the end of the 21st century in this model because of its low transient climate response and the near-cancellation between large regional changes in the hydrologic and ecosystem responses. Analysis of our results in the context of comparable models suggests that destabilization of the tropical land sink is qualitatively robust, although its degree is uncertain.

carbon dioxide | climate change | land carbon sink | ocean carbon sink

The degree of climate warming is determined by the radiative forcing and feedback processes in the climate system. Given a fossil fuel CO_2 emission, the level of CO_2 in the atmosphere, and hence the radiative forcing, depends on the efficiencies of the land and oceans in absorbing the excess CO_2. These efficiencies themselves change with climate and with atmospheric CO_2 levels, so that the carbon cycle represents a critical feedback mechanism in the climate system. The first 19th to 21st century experiments of the response of two coupled carbon–climate models to similar fossil fuel emission scenarios show that their atmospheric CO_2 level, and hence climate warming, differ dramatically by almost 200 parts per million by volume (ppmv) and 2 K by 2100 (1, 2). The differences arise not only because of the different climate sensitivities of the models, but also because of the differences in land and ocean uptake characteristics and hence feedbacks between the carbon and climate systems (3).

Here, we present and analyze a suite of transient experiments (1820–2100) from a new, coupled global carbon–climate model (unpublished work) developed in the framework of the National Center for Atmospheric Research (NCAR) Community Climate System Model (CCSM) (4). We focus primarily on the global carbon–climate feedbacks and the biogeochemical mechanisms that amplify or diminish physical climate change.

Carbon–Climate Model and Experiments

The physical climate core of the coupled carbon–climate model is a modified version of NCAR CSM1.4, which consists of atmosphere, land, ocean, and ice components that are coupled via a flux coupler (5, 6). Into CSM1.4 are embedded a modified version of the terrestrial biogeochemistry model CASA (Carnegie–Ames–Stanford Approach), termed CASA′ (7), and a modified version of the OCMIP-2 (Ocean Carbon Intercomparison Project 2) oceanic biogeochemistry model (8, 9). The coupled carbon–climate model is summarized in *Supporting Text*, which is published as supporting information on the PNAS web site (unpublished work).

CASA′ follows the life cycles of plant functional types from carbon assimilation via photosynthesis, to mortality and decomposition, and the return of CO_2 to the atmosphere via microbial respiration. There are three live vegetation pools and nine soil pools, and the rates of carbon transfer among them are climate-sensitive (10, 11). The carbon cycle is coupled to the water cycle via transpiration and to the energy cycle via dynamic leaf phenology (and hence albedo). A terrestrial CO_2 fertilization effect is possible in the model because carbon assimilation via the Rubisco enzyme is limited by internal leaf CO_2 concentrations; net primary productivity (NPP) thus increases with external atmospheric CO_2 concentrations, eventually saturating at high CO_2 levels.

The ocean biogeochemical model includes in simplified form the main processes for the solubility carbon pump, organic and inorganic biological carbon pumps, and air–sea CO_2 flux. New/export production is computed prognostically as a function of light, temperature, and phosphate and iron concentrations. A fully dynamic iron cycle also has been added, including atmospheric dust deposition/iron dissolution, biological uptake, vertical particle transport, and scavenging.

Control experiments of CSM1 (without an interactive carbon cycle and with atmospheric CO_2 fixed at 280 ppmv) display stable surface temperatures and minimal deep ocean drift without requiring surface heat or freshwater flux adjustments. In benchmark studies, the transient climate response (TCR), i.e., temperature increase at the time of doubling of CO_2 when climate models are forced by a 1% yr^{-1} increase in CO_2, is 1.4 K for the NCAR CSM1 (12).

In the fully coupled carbon–climate model, atmospheric CO_2 is a prognostic variable and is predicted as the residual after carbon exchanges with the land and ocean. A suite of transient experiments (1820–2100) has been conducted with the resulting coupled climate–carbon cycle model, carbon-CSM1.4 (Table 1). The experiments branch off at year 100 from a stable, 1,000-year preindustrial control carbon–climate experiment (global mean annual surface temperature, 13.8 ± 0.1°C; atmospheric CO_2, 283 ± 1.2 ppmv) (unpublished work). The experiments are forced by specifications of fossil fuel CO_2 emission, with historical emission trajectory for the 19th and 20th centuries (13–15) and two fossil fuel emission scenarios for the 21st century: Special Report on Emission Scenarios (SRES) A1B, the "balanced energy sources" scenario; and SRES-A2, the "business-as-usual" scenario (16, 17). These scenarios represent low and high estimates of emissions. No other greenhouse gases or perturbations to the radiative forcing are included. For the SRES-A2 emission scenario, we have carried out a pair of experiments bounding CO_2 fertilization of terrestrial photosynthesis; the biogeochemical CO_2 is set to be either the evolving CO_2 concentration in the lowest 60 mbar (1 bar = 100 kPa) of the atmosphere, or 280 ppmv. The global distribution of plant functional types remains time-invariant throughout all of the experiments. Carbon sources associated with anthropogenic

Freely available online through the PNAS open access option.

Abbreviations: NCAR, National Center for Atmospheric Research; NPP, net primary productivity; pCO_2, CO_2 partial pressure; PgC, petagrams of carbon; ppmv, parts per million by volume; TCR, transient climate response.

†To whom correspondence should be addressed. E-mail: inez@atmos.berkeley.edu.

Table 1. Summary of experiments with the NCAR carbon-CSM1.4

Experiment	Fossil fuel emission	Radiative CO_2	CO_2 for land photosynthesis	CO_2 for air–sea exchange	Carbon–climate coupling
Ctl_ROL	None	Prognostic	Prognostic	Prognostic	Yes
H_ROL	Historical	Prognostic	Prognostic	Prognostic	Yes
H_OL	Historical	283 ppmv	Prognostic	Prognostic	—
H_RO	Historical	Prognostic	280 ppmv	Prognostic	Yes
H_O	Historical	283 ppmv	280 ppmv	Prognostic	—
A1B_ROL	SRES-A1B	Prognostic	Prognostic	Prognostic	Yes
A1B_OL	SRES-A1B	283 ppmv	Prognostic	Prognostic	—
A2_ROL	SRES-A2	Prognostic	Prognostic	Prognostic	Yes
A2_OL	SRES-A2	283 ppmv	Prognostic	Prognostic	—
A2_RO	SRES-A2	Prognostic	280 ppmv	Prognostic	Yes
A2_O	SRES-A2	283 ppmv	280 ppmv	Prognostic	—

Experiments are designated with the prefix ''Ctl'' for the control, ''H'' for the historical fossil fuel emissions for the 19th and 20th centuries, and ''A1B'' or ''A2'' for the SRES fossil fuel emission scenarios for the 21st century. The suffix ''R'' denotes that radiative CO_2 in the atmosphere is given by the column average of the atmospheric CO_2 resulting from the interactive carbon cycle; and the suffices ''L'' and ''O'' denote that the land and ocean carbon cycles are forced by the evolving CO_2 in the lowest 60 mbar of the atmosphere.

land use modification are not included in these experiments. Because the other radiative forcing nearly cancels in the 19th and 20th centuries (18), the climate simulation should be broadly comparable to that observed in the globally averaged sense. However, over the 19th and 20th centuries, land-use modification accounts for ~35% of the cumulative anthropogenic source of atmospheric CO_2. Thus, the modeled atmospheric CO_2 concentrations cannot be directly compared with that observed for a particular year.

Results

We focus our analysis on the changing carbon cycle, because the climate response to a changing CO_2 abundance in the atmosphere follows principally from the climate sensitivity of the physical climate model. We shall use the notation $\Delta\chi$ to denote a temporal change of χ in an experiment and the notation $\delta\chi$ to denote the departure of χ in an experiment with carbon–climate coupling from that without (ROL − OL or RO − O in the notation defined in Table 1). In experiments without carbon–climate coupling, the radiatively active CO_2 is specified to be 283 ppmv, that of the control run, and the increasing CO_2 concentration forces changes in the land and ocean carbon cycles. There are small temperature changes in the experiments without radiative CO_2 carbon–climate coupling relative to the control, because of natural variability and differences in albedo and evapotranspiration due to vegetative processes responding to elevated atmospheric CO_2.

Global Budgets. The cumulative emission of fossil fuel CO_2 is 276 petagrams of carbon (PgC) for the 19th and 20th centuries and 1,380 and 1,732 PgC for the 21st century for emission scenario SRES-A1B and SRES-A2, respectively. ΔCO_2 at the end of the three centuries would be 825 and 993 ppmv, for A1B and A2 scenarios, respectively, if all of the CO_2 remained airborne. The globally averaged changes in surface air temperature (T_{air}) and carbon budgets for the historical and 21st century experiments are summarized in Table 2.

The historical experiments for fossil fuel CO_2 emission show a reasonable simulation of the carbon budget, with globally averaged column CO_2 increasing from 282 ppmv in 1820 to ~345 ppmv with CO_2 fertilization on land (H_ROL). The simulated CO_2 is lower than that observed for 2000 AD because the experiments did not include land-use modification, whose cumulative emission is approximately half that of fossil fuel emission over this period. Globally averaged surface air temperature (ΔT_{air}) increases by 0.3–0.4 K in H_ROL, which is barely

Table 2. Cumulative carbon budgets for the 19th to 21st centuries

Experiment	ΔT, K	Atmospheric CO_2 at end of period, ppmv	Airborne fraction, %	Land fraction, %	Ocean fraction, %
		1820–2000 A.D.			
H_ROL	0.35	345	49	29	22
H_OL	(0.18)*	343	47	31	22
H_RO	0.48	373	70	−3	33
H_O	(0.06)*	372	69	−2	33
		2001–2100 A.D.			
A1B_ROL	1.21	661	48	28	24
A1B_OL	(−0.12)*	647	47	29	24
A2_ROL	1.42	792	54	25	21
A2_OL	(0.12)*	773	52	26	22
A2_RO	1.79	997	76	−2	26
A2_O	(−0.13)*	970	73	0	27

Cumulative fossil fuel emission is 276 PgC for the 19th and 20th centuries. Cumulative fossil fuel emission for the 21st century is 1,380 PgC and 1,732 PgC for SRES-A1B and SRES-A2, respectively. ΔT (column 2) is the difference in global 5-yr mean surface air temperature between the end of the period and the beginning of the period. *Not statistically significant. 1 σ = 0.1 K from Ctl_ROL.

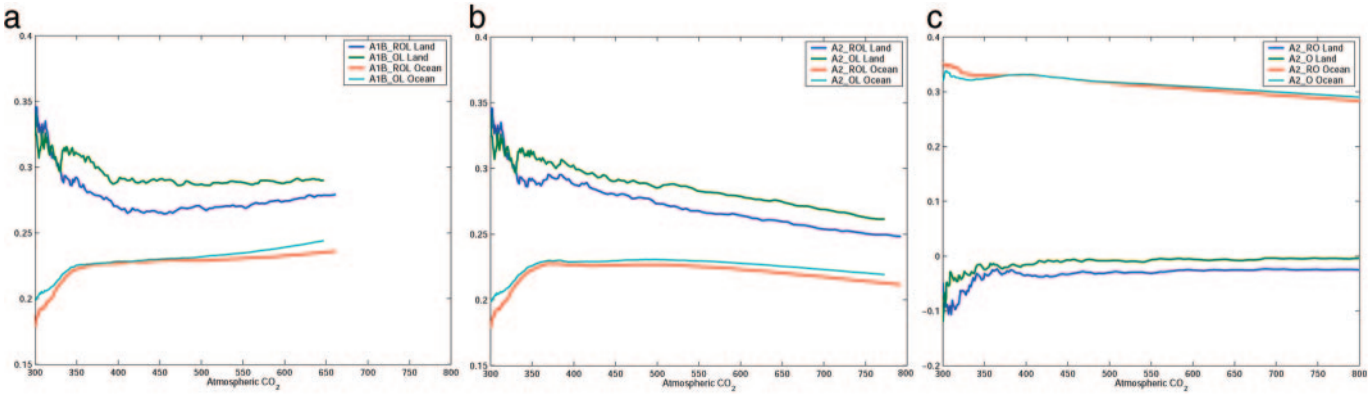

Fig. 1. Evolution of f_{land} and f_{ocn}, the cumulative land and ocean sinks expressed as fractions of the cumulative emission, plotted against atmospheric CO_2 (in ppmv). Data are shown for experiments A1B_ROL and A1B_OL (*a*), A2_ROL and A2_OL (*b*), and A2_RO and A2_O (*c*).

significant statistically (one standard deviation is 0.1 K in the control experiment Ctl_ROL). As can be expected from studies of the contemporary carbon cycle, the climate change over the 19th and 20th century is too small to significantly impact the carbon cycle, so that the partitioning of carbon among the atmosphere, land, and ocean reservoirs is approximately the same with and without carbon–climate coupling, with the airborne fraction hovering around 50% with a CO_2 fertilization sink on land.

In experiments H_RO and H_O, there is no land sink for fossil fuel CO_2. Both the oceans and the atmosphere increase their fossil fuel fractions, and ΔT_{air} increases accordingly. The airborne fraction of 70% without a land sink is higher than is observed for this period.

Fig. 1 shows the evolution, versus global mean atmospheric CO_2 concentration, of f_{land} and f_{ocn}, the cumulative land and ocean carbon sinks expressed as fractions of the cumulative emission for the three pairs of experiments: A1B_ROL and A1B_OL; A2_ROL and A2_OL; and A2_RO and A2_O. Fossil fuel emission in SRES scenario A1B increases until 2050 AD and decreases thereafter, whereas that in A2 increases exponentially over the period. With increasing rates of emission in A2, carbon sequestration processes on land and in the ocean cannot keep up with the emissions, because they have longer time constants than the emission. Furthermore, the capacities of the sinks diminish with increasing CO_2, so that both f_{land} and f_{ocn} decrease with increasing CO_2 in the atmosphere. The A1B emission rate is slower in comparison, so that the mixing of excess of carbon into the deep ocean can maintain a surface ocean CO_2 partial pressure (pCO_2) increase that is slower than that in the atmosphere, and f_{ocn} steadily increases.

Table 2 shows the bulk sink fractions for the experiments for the historical period and for the 21st century. With the land sink operating, f_{land} is ~30% in the historical experiments for the 19th and 20th centuries and ~28% in the A1B experiments and ~25% in the A2 experiments for 21st century, showing that the land sink cannot catch up with the fossil fuel emissions, even in this hypothetical case with no nutrient and other limitations on CO_2 fertilization. In the A1B experiments, the oceans partially make up for the reduced land uptake, so that the airborne fractions ($= 1 - f_{land} - f_{ocn}$) are similar to those in the historical experiments (46–48%). In the A2 experiments with or without carbon–climate coupling, the oceans actually decrease, albeit by only ~1%, their uptake fraction in the 21st century compared to the historical period: The higher rate of CO_2 increase in the atmosphere is not matched by the rate of excess CO_2 removal out of the mixed layer. As a result of the reduced land and ocean uptake fractions, the airborne fraction in the 21st century (52–54%) is higher with the higher fossil fuel emission than that in the 19th and 20th centuries (46–48%). In experiments without the land sink (A2_RO and A2_O), f_{ocn} is higher than that in experiments with the land sink (A2_ROL and A2_OL) because of the higher CO_2 in the atmosphere.

Contrary to results from similar coupled carbon–climate experiments (1, 2, 19–21), this model yields only a very small difference in global carbon budgets (δCO_2 ~ 15–20 ppmv) whether carbon–climate coupling is included or not. Both f_{land} and f_{ocn} are reduced with carbon–climate coupling, although δf_{land} and δf_{ocn} are small, about −1–2%. The causes for relatively similar partitioning of anthropogenic CO_2 with and without carbon–climate coupling are investigated in detail below.

Ocean Carbon Sink. Greenhouse warming influences the oceanic carbon cycle indirectly through changes in ocean circulation and air–sea exchange of CO_2. The magnitude of the ocean carbon sink depends on several competing effects on the CO_2 partial pressure difference across the air–sea interface. Warming reduces solubility and increases pCO_2 in the mixed layer. Warming (and freshening) increases ocean stratification, reduces vertical mixing, and slows the thermohaline circulation, leading to slower removal of excess carbon from the surface ocean. Increased stratification reduces the delivery of nutrients and inorganic carbon to the euphotic zone in most regions and lowers biological productivity. The resultant pCO_2 in the mixed layer decreases if the reduction in carbon supply exceeds the reduction in biological consumption and export. The accumulation of CO_2 in the ocean decreases pH and shifts carbonate chemistry to higher dissolved CO_2 gas fractions. Finally, for the same fossil fuel emission, atmospheric CO_2 levels and air–sea pCO_2 difference increase if the land carbon sink decreases.

In A2_ROL, sea surface temperature at year 2100 is higher by 1.2 K, North Atlantic overturning is slower by 17%, and the export carbon flux is smaller by 5% compared with A2_OL. Their combined effects on ocean carbon uptake is shown in Fig. 2*a*, the difference in the column inventory of total inorganic carbon near the end of the 21st century between experiments A2_ROL and A2_OL at atmospheric CO_2 concentration of 765 ppmv (2094–2098 AD in A2_ROL and 2096–2100 AD in A2_OL). Globally, the cumulative inventory in excess carbon in Fig. 2*a* is lower by ~20 PgC in A2_ROL relative to A2_OL. Circulation effects are most evident in the lower carbon inventory in the subpolar/polar North Atlantic, but reductions occur also in the tropical north Indo-Pacific and Southern Ocean and Antarctic coast, where excess CO_2 enters the oceans, and in the western Atlantic along the path of North Atlantic Deep Water. In the temperate Northern Hemisphere, declines in the upward

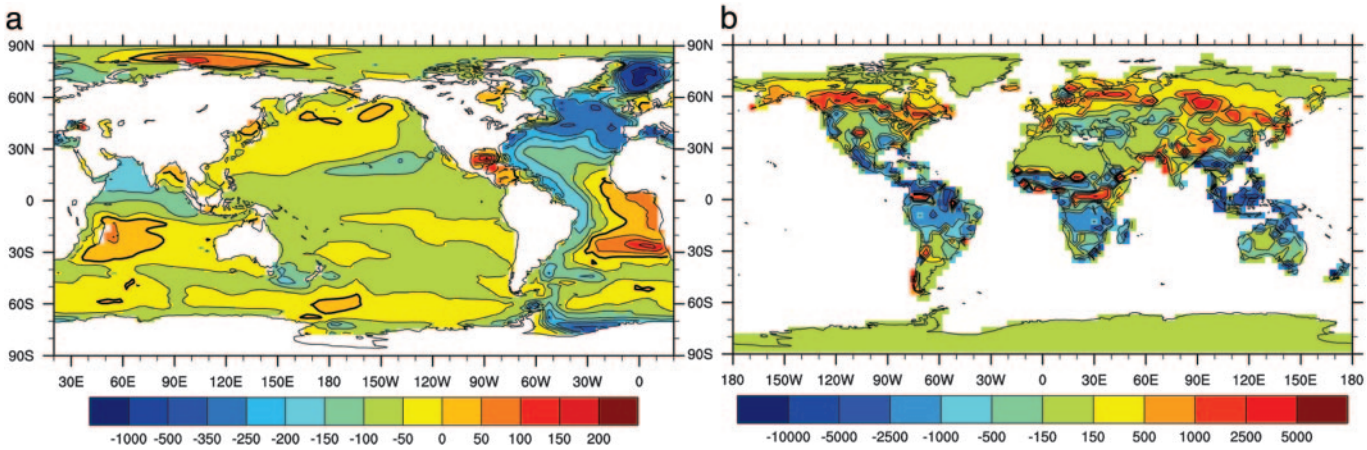

Fig. 2. The impact of carbon–climate feedback on carbon storage. (*a*) Difference in column inventory of dissolved inorganic carbon between experiments A2_ROL and A2_OL due to effects of changing ocean circulation and ocean biogeochemistry. The inventories are averaged over times when the atmospheric CO_2 mixing ratio is 765 ppmv (i.e., 2094–2098 AD in A2_ROL and 2096–2100 in A2_OL). (*b*) Like *a*, but for terrestrial carbon inventory. Unit is gC/m^2.

transport of carbon and nutrients to the surface layer lead to reduced biological production and surface phosphate (data not shown); the net biological effect is to lower surface pCO_2 and increase ocean uptake, thus partially compensating for the slower physical circulation. Integrated production in the Southern Ocean remains about the same, although it tends to shift poleward because of a change in ocean upwelling patterns.

Land Carbon Sink. The cumulative land sinks in the transient experiments result from the differing sensitivities of NPP and respiration to changes in CO_2, light, temperature, and moisture regimes, and their competitive effects on carbon inventory in vegetation and soils. In general, warming and moistening would accelerate NPP and increase vegetation biomass, and would shorten the turnover time of soils.

For both A1B and A2 emission scenarios, the CO_2 fertilization sink on land is only slightly lower, by ~20 PgC, in the experiments with carbon–climate coupling than in those without (Table 2). For experiments without CO_2 fertilization (A2_RO and A2_O), the land acts as a small net source to the atmosphere with carbon–climate coupling. This result is very different from those of other similar models (1–3, 20, 21), in which climate feedbacks lead to massive destabilization of the land sink. Here, we focus on the experiments with the higher emission scenario (A2) and hence greater potential for carbon–climate feedback. Experiment A2_OL shows a cumulative net flux (or biomass increase) of 445 PgC into the biosphere in the 21st century, because there is CO_2 fertilization. The effect of carbon–climate coupling on the land sink is shown as δBiomass (sum of vegetation and soil carbon pools) at an atmospheric CO_2 concentration of 765 ppmv (Fig. 2*b*). Compared with A2_OL, A2_ROL has less uptake in the tropics and greater uptake in high latitudes, so that globally there is little change between the two experiments.

Soil moisture is the difference between precipitation and temperature-dependent evapotranspiration. With warm climates, the demand for moisture exceeds the supply even though there may be an increase in rainfall, so that there is a tendency in the model for warming to lead to drier regimes in warm regions (tropics, summer) and to wetter regimes in cold regions (Fig. 3*a*). The consequence of these differing hydrologic regimes is seen in Fig. 3*b*, the regression of annual mean δNPP against annual mean $\delta T_{air.}$ At low latitudes, the regression coefficient is negative; i.e., NPP is lower in the warmer world because of soil dessication. At middle to high latitudes, NPP is higher in A2_ROL compared with A2_OL because of more favorable

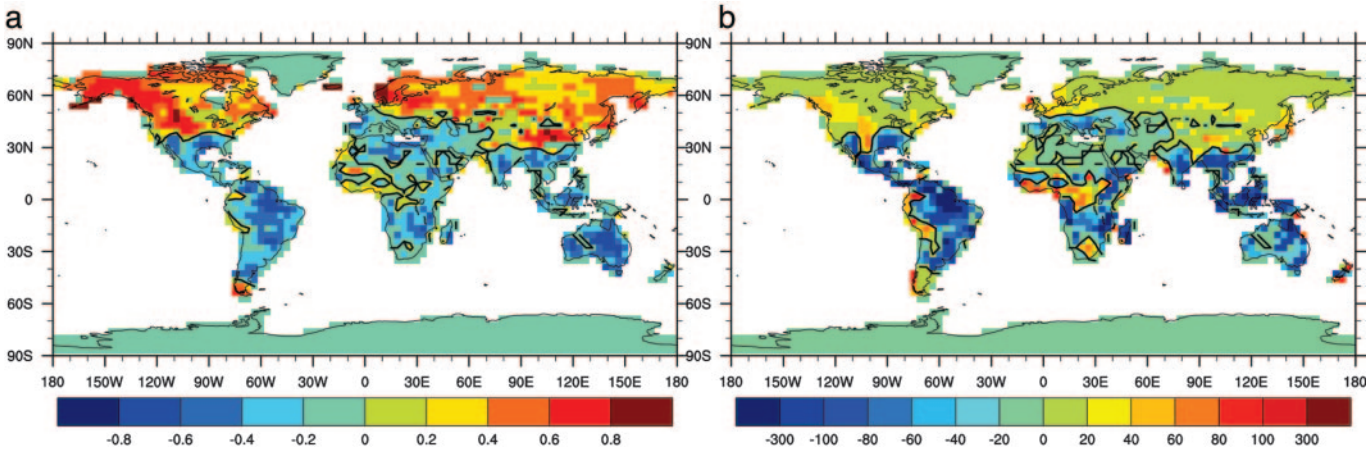

Fig. 3. Regional differences in the change in hydrologic regime and ecosystem productivity with global warming. (*a*) Correlation between annual mean δT_{air} and $\delta\beta_{iran}$ for the 21st century. β_{iran} is an index (between 0 and 1) of soil moisture saturation. (*b*) Regression (in kgC/m^2 per yr per K) of annual mean δNPP against annual mean δT_{air}. δ is defined as the difference between experiments A2_ROL and A2_OL for the 21st century.

climate. The effects of decreased NPP in the tropics lead to smaller vegetation and soil carbon pools, which, when combined with the faster decomposition rate, yield lower carbon storage. Thus, there is local competition between temperature and moisture in determining the carbon source/sink strength, with significant regional cancellation in net carbon storage between the tropics and high latitudes.

Discussion and Summary

Experiments with the carbon–climate model NCAR carbon-CSM1.4 show that the land and oceans decrease their capacity to act as repositories of fossil fuel CO_2 as fossil fuel CO_2 emissions accelerate and greenhouse warming progresses. In terms of global budgets, the model yields minimal difference between experiments with and without carbon–climate coupling, compared with δCO_2 of 280 and 80 ppmv for the Hadley Centre model (1) and Institut Pierre-Simon Laplace (IPSL) model (2), respectively, because of the weaker carbon–climate coupling in the NCAR carbon-CSM1.4. To begin with, the TCR is 1.4 K for NCAR CSM1 (12), at the low end of the range 1.1–3.1 K for climate models (17). The magnitude of the ocean carbon sink to carbon–climate feedbacks depends on the representation of ocean circulation in the physical climate model (22, 23) and its response to changing climate, as well as on the sensitivity of marine ecosystem processes to the changing ocean climate (24, 25). The NCAR carbon-CSM1.4 has a stronger fossil fuel CO_2 uptake (and a lower airborne CO_2 fraction) with the control climate than, for example, the Hadley model, and this sets the stage for weaker coupling between the carbon–climate systems.

The magnitude of the land carbon sink and its response to carbon–climate feedbacks depend on the turnover times of the carbon pools, the sensitivity of terrestrial processes to climate change, and the transient climate and hydrologic response of the physical climate model. The turnover time of vegetation and soil carbon, or the lag between photosynthesis and respiration, determines to the lowest order the magnitude of the carbon sink itself. TRIFFID, the dynamic vegetation model in ref. 1, whose single soil carbon pool has a turnover time of 25 years, thus has potentially a greater carbon storage capacity than CASA′, which has nine soil carbon pools and a turnover time of <5 years for $\sim$60% of the soil carbon flux. The shorter turnover time is consistent with flux-weighted times derived from ^{14}C measurements (26). Intercomparison of six ecosystem models shows that TRIFFID also has the steepest photosynthesis and respiration increase in response to specified 19th to 21st century climate change and CO_2 increase (27). Multiplying this high ecosystem sensitivity is the high TCR (3.5 K) of the climate model HadCM3, so that the coupled carbon–climate model yields, by 2050, tropical temperatures above the optimal temperature for photosynthesis. The excess heating drives the dieback of the rainforest, accelerates soil carbon loss, and transforms the land from a sink to a source of carbon for the atmosphere (28). In the IPSL model, with an intermediate TCR of $\sim$2 K, the reduction in photosynthesis due to warming and drying in the tropics exceeds the increase in photosynthesis due to lengthening of the growing season at high latitudes, so that there is a net reduction in the strength of the global land sink (29). In the NCAR carbon-CSM1.4, the climate and ecosystem changes are qualitatively similar to that in the IPSL model. However, with the low TCR of 1.4 K, the decrease in carbon sink at low latitudes nearly cancels the increase at high latitude, with little change in the global net land sink in the NCAR carbon-CSM1.4. The temperature increases are below the threshold values for vegetation dieback.

Although there are observations of precipitation trends, there is a paucity of observations of soil moisture, especially in the tropics, to permit quantification of the competitive and/or synergistic effects of temperature and hydrologic changes on photosynthesis and respiration. Satellite and site data also show that interannual and interdecadal variations in biological productivity are sensitive to variations in the hydrologic regime as well as to variations in temperature (30–35), and so the increasing destabilization of the terrestrial carbon sink with warming and drying as modeled by coupled carbon–climate models such as presented here is qualitatively plausible, even though the timing is uncertain. The timing would also depend, *inter alia*, on other climate forcing and processes not included here, e.g., dynamic vegetation, high-latitude peatlands, and ocean acidification.

We thank the NCAR Community Climate System Model Team, in particular J. Kiehl, W. Collins, G. Bonan, P. Gent, and P. Rasch, for support and assistance. Ed Sarachik provided critical comments on the manuscript. Computations were carried out at NCAR and the National Energy Research Scientific Computing Center. This work was supported by National Science Foundation (NSF) Grant NSF ATM-9987457, National Aeronautics and Space Administration (NASA) EOS-IDS Grant NAG5-9514, NASA Carbon Cycle Program Grant NAG5-11200, the Laboratory Directed Research and Development Program of the Lawrence Berkeley National Laboratory, and the Ocean and Climate Change Institute of the Woods Hole Oceanographic Institution. The NCAR is sponsored by the NSF. This is Woods Hole Oceanographic Institution contribution 11389.

1. Cox, P. M., Betts, R. A., Jones, C. D., Spall, S. A. & Totterdell, I. J. (2000) *Nature* **408,** 184–187.
2. Dufresne, J. L., Friedlingstein, P., Berthelot, M., Bopp, L., Ciais, P., Fairhead, L., Le Treut, H. & Monfray, P. (2002) *Geophys. Res. Lett.* **29,** 10.1029/2001GL013777.
3. Friedlingstein, P., Dufresne, J. L., Cox, P. M. & Rayner, P. (2003) *Tellus Ser. B* **55,** 692–700.
4. Blackmon, M., Boville, B., Bryan, F., Dickinson, R., Gent, P., Kiehl, J., Moritz, R., Randall, D., Shukla, J., Solomon, S., *et al.* (2001) *Bull. Am. Meteorol. Soc.* **82,** 2357–2376.
5. Boville, B. A., Kiehl, J. T., Rasch, P. J. & Bryan, F. O. (2001) *J. Climate* **14,** 164–179.
6. Boville, B. A. & Gent, P. R. (1998) *J. Climate* **11,** 1115–1130.
7. Randerson, J. T., Thompson, M. V., Conway, T. J., Fung, I. Y. & Field, C. B. (1997) *Global Biogeochem. Cycles* **11,** 535–560.
8. Doney, S. C., Lindsay, K. & Moore, J. K. (2003) *Ocean Biogeochemistry: The Role of the Ocean Carbon Cycle in Global Change*, ed. Fasham, M. J. R. (Springer, Berlin), pp. 217–238.
9. Najjar, R., Sarmiento, J. & Toggweiler, J. R. (1992) *Global Biogeochem. Cycles* **6,** 45–76.
10. Dickinson, R. E., Shaikh, M., Bryant, R. & Graumlich, L. (1998) *J. Climate* **11,** 2823–2836.
11. Friedlingstein, P., Joel, G., Field, C. B. & Fung, I. Y. (1999) *Global Change Biol.* **5,** 755–770.
12. Meehl, G. A., Collins, W. D., Boville, B., Kiehl, J. T., Wigley, T. M. L. & Arblaster, J. M. (2000) *J. Climate* **13,** 1879–1898.
13. Andres, R. J., Fielding, D. J., Marland, G., Boden, T. A., Kumar, N. & Kearney, A. T. (1999) *Tellus Ser. B* **51,** 759–765.
14. Marland, G. & Rotty, R. M. (1984) *Tellus Ser. B* **36,** 232–261.
15. Andres, R. J., Marland, Fung, I. & Matthews, E. (1996) *Global Biogeochem. Cycles* **10,** 419–429.
16. Nakicenovic, N., Alcamo, J., Davis, G., de Vries, B., Fenhann, J., Gaffin, S., Gregory, K., Grubler, A., Yong Jung, T., Kram, T., *et al.* (2000) *Special Report on Emission Scenarios* (Cambridge Univ. Press, Cambridge, U.K.).
17. Houghton, J. T., Ding, Y., Griggs, D. J., Noguer, M., van der Linden, P. J., Dai, X., Maskell, K. & Johnson, C. A., eds. (2001) *Climate Change 2001: Synthesis Report* (Cambridge Univ. Press, Cambridge, U.K.).
18. Hansen, J., Sato, M., Nazarenko, L., Ruedy, R., Lacis, A., Koch, D., Tegen, I., Hall, T., Shindell, D., Santer, B., *et al.* (2002) *J. Geophys. Res. Atmospheres* **107,** 10.1029/2001JD001143.
19. Zeng, N., Qian, H. F., Munoz, E. & Iacono, R. (2004) *Geophys. Res. Lett.* **31,** 10.1029/2004GL020904.
20. Thompson, S. L., Govindasamy, B., Mirin, A., Caldeira, K., Delire, C., Milovich, J., Wickett, M. & Erickson, D. (2004) *Geophys. Res. Lett.* **31,** 10.1029/2004GL021239.
21. Govindasamy, B., Thompson, S., Mirin, A., Wickett, M., Caldeira, K. & Delire, C. (2005) *Tellus Ser. B* **57,** 153–163.

22. Matsumoto, K., Sarmiento, J. L., Key, R. M., Aumont, O., Bullister, J. L., Caldeira, K., Campin, J. M., Doney, S. C., Drange, H., Dutay, J. C., *et al.* (2004) *Geophys. Res. Lett.* **31,** 10.1029/2003GL018970.
23. Doney, S. C., Lindsay, K., Caldeira, K., Campin, J. M., Drange, H., Dutay, J. C., Follows, M., Gao, Y., Gnanadesikan, A., Gruber, N., *et al.* (2004) *Global Biogeochem. Cycles* **18,** 10.1029/2003GB002150.
24. Sarmiento, J. L., Slater, R., Barber, R., Bopp, L., Doney, S. C., Hirst, A. C., Kleypas, J., Matear, R., Mikolajewicz, U., Monfray, P., *et al.* (2004) *Global Biogeochem. Cycles* **18,** 10.1029/2003GB002134.
25. Lefevre, N., Watson, A. J., Olsen, A., Rios, A. F., Perez, F. F. & Johannessen, T. (2004) *Geophys. Res. Lett.* **31,** 10.1029/2003GL018957.
26. Trumbore, S. (2000) *Ecol. Appl.* **10,** 399–411.
27. Cramer, W., Bondeau, A., Woodward, F. I., Prentice, I. C., Betts, R. A., Brovkin, V., Cox, P. M., Fisher, V., Foley, J. A., Friend, A. D., *et al.* (2001) *Global Change Biol.* **7,** 357–373.
28. Cox, P. M., Betts, R. A., Collins, M., Harris, P. P., Huntingford, C. & Jones, C. D. (2004) *Theor. Appl. Climatol.* **78,** 137–156.
29. Berthelot, M., Friedlingstein, P., Ciais, P., Monfray, P., Dufresne, J. L., Le Treut, H. & Fairhead, L. (2002) *Global Biogeochem. Cycles* **16,** 10.1029/2001GB001827.
30. Angert, A., Tucker, C. J., Biraud, S., Bonfils, C., Henning, C. C., Buermann, W. & Fung, I. (2005) *Proc. Natl. Acad. Sci. USA*, in press.
31. Bonfils, C., Angert, A., Henning, C., Biraud, S., Doney, S. C. & Fung, I. (2005) *Geophys. Res. Lett.* **32,** 10.1029/2005GL22583.
32. Nemani, R., White, M., Thornton, P., Nishida, K., Reddy, S., Jenkins, J. & Running, S. (2002) *Geophys. Res. Lett.* **29,** 10.1029/2002GL014867.
33. Nemani, R. R., Keeling, C. D., Hashimoto, H., Jolly, W. M., Piper, S. C., Tucker, C. J., Myneni, R. B. & Running, S. W. (2003) *Science* **300,** 1560–1563.
34. Huxman, T. E., Smith, M. D., Fay, P. A., Knapp, A. K., Shaw, M. R., Loik, M. E., Smith, S. D., Tissue, D. T., Zak, J. C., Weltzin, J. F., *et al.* (2004) *Nature* **429,** 651–654.
35. Weltzin, J. F., Loik, M. E., Schwinning, S., Williams, D. G., Fay, P. A., Haddad, B. M., Harte, J., Huxman, T. E., Knapp, A. K., Lin, G. H., *et al.* (2003) *Bioscience* **53,** 941–952.